SCIENTIFIC REPORTS

OPEN

SUBJECT AREAS:
SYNTHESIS AND PROCESSING
SURFACES, INTERFACES AND THIN FILMS

Received
30 October 2013

Accepted
24 March 2014

Published
10 April 2014

Correspondence and requests for materials should be addressed to P.V.S. (satyam@iopb.res.in; pvsatyam22@gmail.com)

* Current address: Department of Materials Science and Engineering, University of Wisconsin-Madison 1509 University Ave, Madison, WI 53706, USA.

Coherently Embedded Ag Nanostructures in Si: 3D Imaging and their application to SERS

R. R. Juluri[1], A. Rath[1]*, A. Ghosh[1], A. Bhukta[1], R. Sathyavathi[2], D. Narayana Rao[2], Knut Müller[3], Marco Schowalter[3], Kristian Frank[3], Tim Grieb[3], Florian Krause[3], A. Rosenauer[3] & P. V. Satyam[1]

[1]Institute of Physics, Sachivalaya Marg, Bhubaneswar, Odisha-751005, India, [2]School of Physics, University of Hyderabad, Hyderabad – 500 046, India, [3]Institute of Solid State Physics, University of Bremen, Otto-Hahn-Allee 1, 28359 Bremen, Germany.

Surface enhanced Raman spectroscopy (SERS) has been established as a powerful tool to detect very low-concentration bio-molecules. One of the challenging problems is to have reliable and robust SERS substrate. Here, we report on a simple method to grow coherently embedded (endotaxial) silver nanostructures in silicon substrates, analyze their three-dimensional shape by scanning transmission electron microscopy tomography and demonstrate their use as a highly reproducible and stable substrate for SERS measurements. Bi-layers consisting of Ag and GeO_x thin films were grown on native oxide covered silicon substrate using a physical vapor deposition method. Followed by annealing at 800°C under ambient conditions, this resulted in the formation of endotaxial Ag nanostructures of specific shape depending upon the substrate orientation. These structures are utilized for detection of Crystal Violet molecules of 5×10^{-10} M concentrations. These are expected to be one of the highly robust, reusable and novel substrates for single molecule detection.

The discovery of Surface Enhanced Raman Scattering (SERS) lead to the solutions for many challenges due to its power as an analytical tool for the sensitive and selective detection of molecules adsorbed on noble metal nanostructures[1–5]. In SERS, enormous field enhancement occurs at the noble metal junctions due to electromagnetic field localization coupling resonantly with the surface plasmon[6–8]. One of the major challenges in the field of SERS is to have an appropriate and effective substrate to take care of low signal enhancement, poor selectivity, unstable and irreproducible signals[5]. Highly reproducible and stable substrates can efficiently be used as SERS based sensors for label free immunoassays[9], biosensing[10] and other applications[5].

The success and the usefulness of the SERS method depends on the optimization of the interaction between adsorbed molecules and the surface plasmonic structures[5]. To maximize the enhancement factors for the SERS signal, various shapes and combinations of gold and silver nanostructures, such as SiO_2-encapsulated gold particles[11], nanorods of Ag deposited using oblique angle vapor deposition[12], 2D Au nano-mushroom arrays[13], polyhedral Ag mesocages[14], and film over nanospheres (FON's)[15] have been tried out and obtained better stability and reproducibility in some cases. Besides plasmonic applications, silver nanostructures can also be used as antennas to convert light into localized electric fields or as wave guides to route light to specified locations with a precision of few nanometers[16], photonic crystals and in infrared polarizers[17,18]. Embedded Ag nanoparticles have been found to enhance the light absorption in semiconductors, due to their strong plasmonic near-field coupling[5]. Owing to the large contingent of applications of Ag nanostructures, it is a challenge to control the shape, size, composition and placement/position of Ag nanostructures. Wiley et al., reported a solution-phase polyol synthesis for controlled shapes of Ag nanostructures, such as, pentagonal nanowires, cuboctahedra, nanocubes, nanobars etc.[19]. Recently we have reported the possibility of growth of endotaxial Ag nanostructures by chemical vapor deposition (CVD) method[20].

In the present work, we report on the growth of various shapes of coherently embedded or/and endotaxial Ag nanostructures on silicon substrates using a physical vapor deposition method (PVD). It is important to know that both the CVD and PVD are two different methods but the yielding endotaxial structures in the both processes indicate an interesting phenomenon of growth. The present paper also presents control over the position and shape of Ag structures by introducing the Ag thin film sandwiching between the GeO_x and SiO_x. Such control is not possible in CVD method. We present a simple process to grow substrate symmetry-driven silver nanostructures on silicon substrate by annealing the samples at ≈800°C in air. The very nature of Ag nanostructures (i.e. embedding

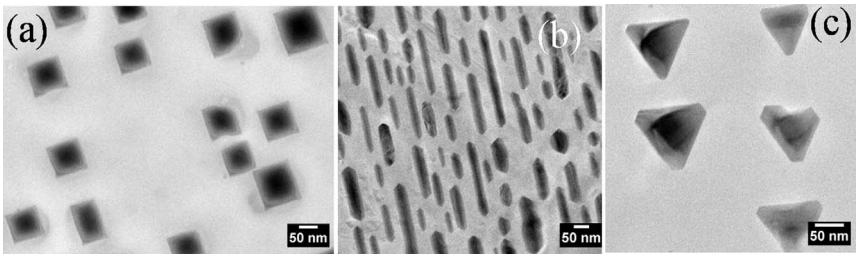

Figure 1 | Planar TEM Micrographs of 2 nm Ag/17 nm GeO_x/SiO_x on (a) Si(100), (b) Si(110) and (c) Si(111) annealed at 800°C in air.

coherently in substrate) would provide a stable substrate for SERS applications. Our results reveal an interesting process involving a low-temperature etching of native oxide of the silicon substrate using GeO_x as an intermediate layer to help the growth of the endotaxial Ag nanostructures. The term "endotaxy" here refers to the growth of precipitate phases in a bulk matrix, with coherent interfaces surrounding the precipitate[21]. We present 3D imaging of these embedded structures using scanning transmission electron microscopy (STEM) based tomography in addition to the use of different procedure of the growth (i.e., PVD). Using traditional gas phase or solution phase methods, formation of various shapes and sizes of Ag nanostructures has been reported, but they are not endotaxial in nature. It is also be noted that, traditionally, endotaxial structures were prepared with molecular beam epitaxy (MBE) in ultra high vacuum conditions (UHV)[22]. Earlier reports indicated that endotaxial structures have potential applications in thermoelectric, magnetic systems, spin polarized contacts, opto-electronic components and nanoelectronics[22].

Results

Growth of Endotaxial Ag nanostructures: a simple PVD method. Using physical vapor deposition and annealing in ambient conditions, we have succeeded in growing the coherently embedded nanostructures of Ag in Si. The results presented in figure 1 depict the shape variation of Ag nanostructures depending on the substrate orientation. For (100), (110) and (111), the surface unit cell has 4 – fold, 2 – fold and 3 – fold symmetry, respectively. The shape of Ag nanostructures is commensurate with the substrate surface symmetry (4, or 2 and 3 fold symmetry for (100), (110) and (111) orientations, respectively) as shown in figure 1. Figure 1 (a) depicts a bright field (BF) planar TEM micrograph for 2 nm Ag/17 nm GeO_x/SiO_x/Si (100) annealed at ≈800°C in air for 30 minutes. This shows formation of square/rectangular shaped silver nano-structures on Si(100) substrate following the four-fold symmetry of the substrate. By considering about 220 particles from many TEM micrographs the average length of the square/rectangle shape Ag nanostructures is found to be 110 nm ± 50 nm and average breadth is 100 nm ± 40 nm with an aspect ratio of 1.1. Also, figure 1 (b) reveals the formation of silver nanorod structures for the 2 nm Ag/17 nm GeO_x/SiO_x/Si (110) annealed at ≈800°C in air for 30 minutes, following the substrate's two-fold symmetry. The average length and width of the rod shaped Ag nanostructures is found to be 150 nm ± 80 nm, 30 nm ± 10 nm with an aspect ratio of ≈ 5.0. From the associated error it is clear that a wide distribution of sizes is observed. Figure 1 (c) is for the 2 nm Ag/17 nm GeO_x/SiO_x/Si (111) annealed at ≈800°C in air for 30 minutes and this reveals the triangular nanostructures formed by following a three-fold symmetry of the Si(111) substrate. The process of Ag diffusion from thin films through the reactive interfaces of GeO_x and SiO_x which resulted in a clean Ag - Si interface is an interesting result from the present measurements.

Figure 2 (a) shows a low magnification cross-sectional TEM (X-TEM) bright field (BF) image of as-deposited 2 nm Ag/17 nm GeO_x/SiO_x/Si(100). This confirms the presence of spherical silver nanoparticles on top of an amorphous GeO_x layer. It should be noted that a physical vapor deposition of Ge in high vacuum condition yielded GeO_x layer. The as-deposited Ag thin film showed isolated irregular nanostructures. From figure 2 (a), the thicknesses of the GeO_x and the native oxide (SiO_x) layers were found to be ≈17 nm and ≈2 nm, respectively. Figure 2 (b) depicts a low magnification BF X-TEM micrograph of 2 nm Ag/17 nm GeO_x/SiO_x/Si (100) at ≈800°C (annealing done in air for 30 minutes). From this micrograph, the thickness of GeO_x is found to be ≈75 nm where SiO_x is ≈20 nm thick. Following the annealing in air, the GeO_x and SiO_x layer thicknesses have been increased by a factor of ≈3.4 and ≈9, respectively. The cross-sectional image taken (for 2 nm Ag/17 nm GeO_x/SiO_x/Si(100) @800°C), shown in figure 2 (b), confirms the intrusion of silver into the silicon substrate. Figure 2 (c) represents a high resolution lattice image of a small area shown in Figure 2 (b). This lattice image confirms the presence of Ag (111) (0.238 ± 0.005 nm) and Si (111) (0.315 ± 0.005 nm) lattice planes as an endotaxial structure. The lattice images depict the presence of Moiré fringes in the structures, which confirms the presence of the coherent embedment nature of silver nanostructures in silicon. The Moiré fringe spacing can be determined by

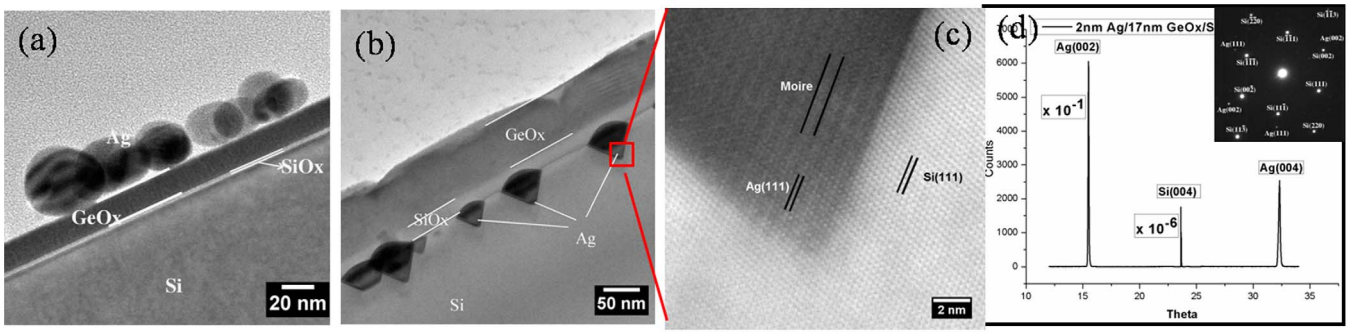

Figure 2 | X-TEM Micrographs of 2 nm Ag/17 nm GeO_x/SiO_x/Si (100) (a) Low Mag of as-deposited (b) Low Mag of 800 °C annealed in air (c) HR-XTEM depicts endotaxial structures (with Moire fringes) and (d) X-Ray Diffraction Pattern showing the single crystalline nature of the Ag nano structures which also complimented by a Selected Area Electron Diffraction (SAD) pattern taken on a single structure.

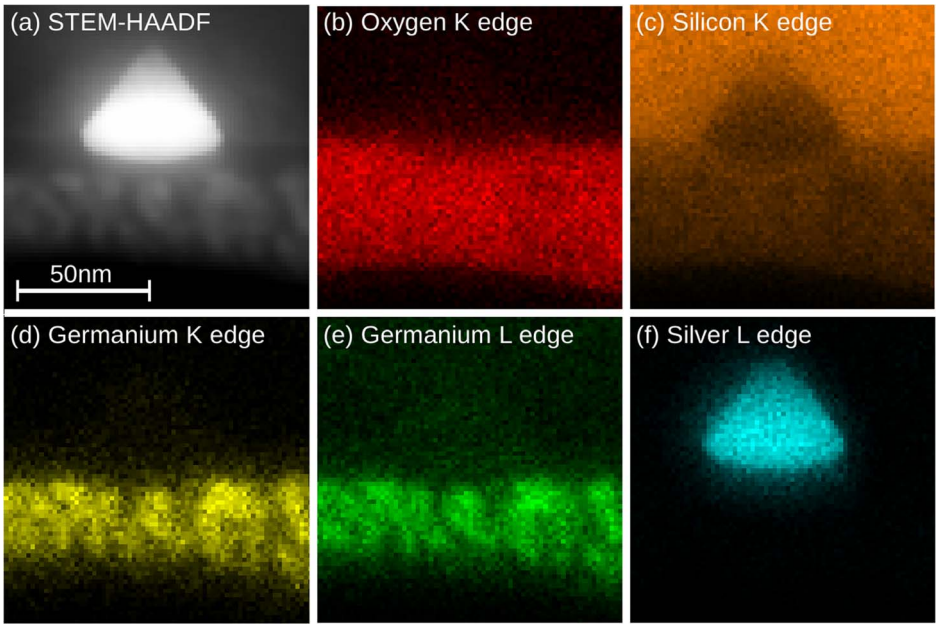

Figure 3 | STEM- EDX Elemental of mapping 2 nm Ag/17 nm GeO_x/SiO_x/Si (100) @800°C (a) STEM Micrograph, (b) Oxygen mapping, (c) Silicon mapping, (d),(e) Germanium K,L mapping and (e) Silver mapping.

$$d_m = d_1 d_2 \Big/ \left((d_1 - d_2)^2 + d_1 d_2 \beta^2\right)^{1/2}$$

where d_1,d_2 are lattice spacings of the planes which are constituents of Moiré fringes and β is the angle between the planes[23]. The Moiré fringe spacing of 0.96 nm was calculated between Ag(111) and Si(111) planes with β = 0. This matches well with the measured fringe spacing from our measurements (Figure 2 (c)) is 0.95 ± 0.01 nm. Figure 2 (d) is the synchrotron XRD spectrum of the 2 nm Ag/17 nm GeO_x/SiO_x/Si(100) @800°C in air for 30 minutes, which depicts the single crystalline nature of the silver nanostructures on silicon (100) substrate. In the XRD spectrum, only Ag(002) and Ag(004) peaks were observed along with the Si(004) peak that belongs to the substrate. Due to the larger x-ray beam size (250 μm × 250 μm), the XRD show the macroscopic ordering. Hence, the XRD data confirms the presence of crystalline Ag structures over a larger scale compared to TEM. The inset of figure 2(d) shows the selected area electron diffraction (SAED) pattern taken on a single endotaxial nanostructure, confirming that the silver nanostructures are single crystalline in nature. XRD and SAED confirm the macroscopic and microscopic coherent nature of the Ag nanostructures, respectively.

Plausible mechanism. We propose a plausible mechanism involved in the enhanced desorption of SiO_x and GeO_x at initial stages[20]. During annealing of the sample, GeO_x desorbs into volatile GeO from the metal edges by forming intermediate solid GeO(s)[24]. It has been reported that GeO desorbs from a solid GeO layer at >300°C[25,26]. In our case, the metal could be a catalyst for the formation of GeO(s) which then desorbs as GeO gas[24].

$$GeO(s) \rightarrow GeO(g) \quad (1)$$

Wang et al. reported the disproportionation of GeO into Ge and GeO_2[27], and they have also shown the formation of crystalline germanium above 600°C annealing.

$$2GeO \rightarrow GeO_2 + Ge \quad (2)$$

Ge formed in the disproportionation of GeO thus has a possibility to react with native SiO_x to form volatile SiO around 750°C. Furthermore, Yun et al., reported the desorption of SiO from SiO_2 in the vicinity of Ge[28]:

$$Ge + 2SiO_2 + Si \rightarrow GeO(g) + 3SiO(g) \quad (3)$$

In a proposed cyclic process the GeO formed in this reaction (3) also disproportionate into GeO_2 and Ge and the Ge will help desorption of SiO_2 into volatile SiO resulting a competition between GeO disproportionation, SiO desorption and SiO_2 formation.

It is well known from literature that silver diffuses into silicon through an interstitial-substitution mechanism[29,30]. Ag diffusion to reach the silicon surface has been enhanced due to desorption of SiO_x and GeO_x. This would presumably happen during annealing. During cooling, initially, oxidation of the silicon substrate occurs which might be a reason for increased thickness of the SiO_x layer, the condensation of GeO_x might take place at a lower temperature compared to SiO_x. The increase of the GeO_x layer is also observed from the cross-sectional TEM micrograph (figure 2(b)) which might be explained through the stochiometric oxide formation.

Chemical analysis and 3D imaging. In order to understand the chemical nature of the system, two-dimensional energy-dispersive x-ray (EDX) analysis of a typical endotaxial structure has been performed in STEM mode as shown in Figure 3. The high-angle annular dark field (HAADF) Z-contrast STEM micrograph in figure 3 (a) depicts the investigated region containing a 50 nm wide pyramidal structure. As shown by the Oxygen map in figure 3(b), the endotaxial structure itself is free of oxides while the presence of oxygen is clearly confirmed in the top two oxide layers. Together with the silicon map in figure 3(c) and the germanium distributions in figures 3(d,e), the first oxide layer from the substrate side is identified as SiO. From the line-profile analysis the EDX signal, the Si signal decreases with increasing silver signal, and that SiO_x is formed at the surface where no Ge is present and is followed by a mixed layer with SiO_x and GeO_x. Moreover, figure 3(c) exhibits a significant silicon deficiency in the endotaxial formation, suggesting the substitution of silicon here. In fact, the silver map in figure 3(f) reveals that the investigated structure consists of silver which is also in agreement with the high Z-contrast observed in the HAADF image (as in figures 3 (a), 4(a)). Together with the SAED pattern shown in figure 2(d), we can preclude the presence of silver silicide because silver and silicon lattice sapcings constitute a

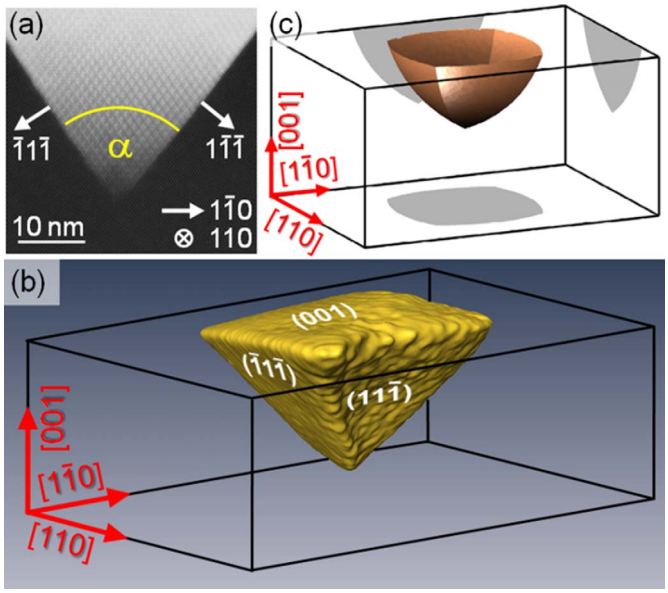

Figure 4 | (a) STEM – HAADF micrograph of 2 nm Ag/17 nm GeO_x/SiO_x/Si(100) @800 C annealed in air, with selected directions indexed from this 2D projection. (b) Reconstructed 3D tomography view of one of the endotaxial islands, showing that the silver embedment is terminated by {111} facets and an (001) base. (c) Result of the Wulff construction, explaining this pyramidal shape and its orientation theoretically in terms of interface energy.

ratio of ¾ which matches with the expectation for the pure materials exactly.

The plane- and cross-sectional TEM studies in figures 1(a) and 2(b,c) already imply that the silver nanostructures obey a pyramidal shape with a quadratic base which has a [100] surface normal. Moreover, figure 4(b) exhibits an angle of $\alpha = 70.0^\circ$ between the projected Ag/Si interface which agrees well with the theoretical angle of 70.5° for {111} facets. However, to prove that the silver nanostructures are indeed terminated by four microscopically flat {111} facets in addition to the quadratic base, STEM tomography has been performed to allow for the 3D reconstruction shown in figure 4(b). This demonstrates the termination by (-11-1) and (11-1) facets in this particular perspective. Finally, we calculated the equilibrium shape of silver embedments in silicon theoretically by considering energies for different crystallographic orientations of the Ag/Si interface. We took the energies from Xin et al.[31], who computed energies for Ag(001)/Si(111), Ag(011)/Si(111) and Ag(111))/Si(111) twisted interfaces. By Wulff's construction[32,33], we then found the terminating facets of the Ag embedments in figure 4(c) for the case that the Ag facets are lying on Si (111) facets. As the shape agrees well with the reconstruction in figure 4(b), we conclude that the observed pyramid formation is driven by Ag/Si interface energy minimization and takes the shape close to thermodynamic equilibrium.

SERS applications. Silver nano square/rectangles formed in the 2 nm Ag/17 nm GeO_x/SiO_x/Si(100) @ 800°C substrate were used to detect the Crystal Violet organic dye molecules. CV is a commonly used molecule for SERS study because of its high Raman scattering cross-section and it chemisorbs on the silver surfaces due to the amino group[3,34,35]. The SERS spectra reveal the characteristic peaks of CV at 1172, 1371, and 1619 cm^{-1} [36]. Figure 5 (a) depicts the SEM micrograph of 2 nm Ag/17 nm GeO_x/SiO_x/Si(100) @ 800°C annealed in air, which was treated with HF for 90 minutes to remove the top oxide layers and expose the Ag nanoparticles in order to use it for SERS. Figure 5 (b) is the corresponding SERS spectra of CV with 5×10^{-10} molar (0.5 nM) concentration drop casted on this HF treated 2 nm Ag/17 nm GeO_x/SiO_x/Si(100) @ 800°C, the same concentration of CV was drop casted on plain silicon in order to compare the enhancement due to the endotaxial square nanostructures. Analytical enhancement factors (AEF) were calculated for the characteristic peaks of crystal violet using the following equation

$$AEF = (I_{SERS}/C_{SERS})/(I_{RS}/C_{RS})$$

The analytical enhancement factors (AEF) for the CV for peak positions of 913, 1172 and 1371 are 1.7×10^7, 1.8×10^7 and 1.8×10^7 respectively, for nanosquare/rectangular structured sample i.e. for 2 nm Ag/17 nm GeO_x/SiO_x/Si(100) @ 800 C annealed in air and HF-treated, where as for as deposited case the AEF's are as follows: 2.9×10^4, 3.0×10^4 and 2.9×10^4, respectively. This enhancement of three (3) orders of magnitude compared to the as-deposited is attributed to the shape and placement of Ag nanostructures. Figure 5(c) SERS spectrum of Crystal Violet on HF treated 2 nm Ag/17 nm GeO_x/SiO_x/Si(100) @ 800°C at different points showing the consistency of the substrate with uniform enhancement. A SERS substrate can be readily obtained as and when required by etching out the oxide layer with HF and use it for SERS recording. In their detailed paper, Le Ru et al., reported average enhancement factor of $\approx 10^5$ for 5 nM CV (page no 13798, Table 2 in ref. 3) for an analyte in a partially aggregated Ag colloid solution. Our average enhancement factor are two orders of magnitude higher than the ones reported for similar concentration CV in reference 3. It should be noted that we

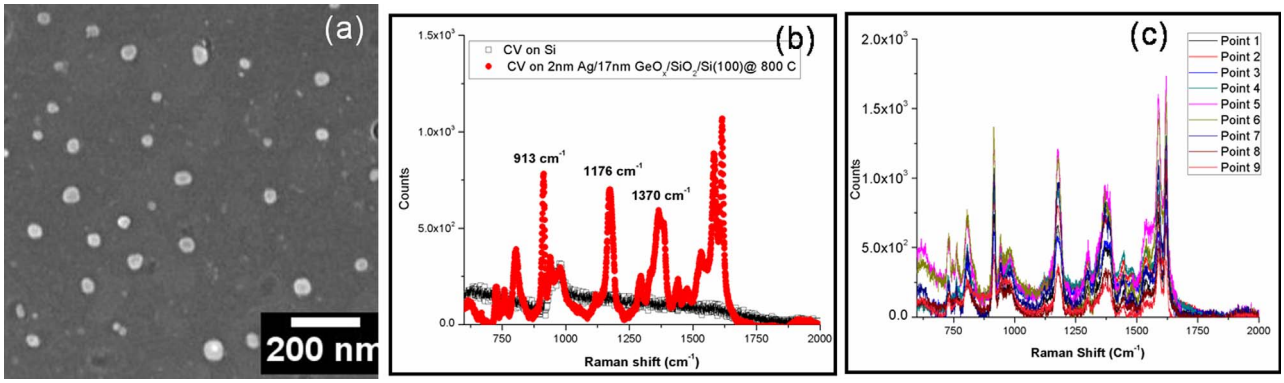

Figure 5 | **(a) SEM Micrographs of 2 nm Ag/17 nm GeO_x/SiO_x/Si(100) @800 °C in air etched with hydro fluoric acid for 90 minutes, (b) SERS spectrum of Crystal Violet with a concentration of 5×10^{-10} Molar drop casted on 2 nm Ag/17 nm GeO_x/SiO_x/Si(100) @800 °C in air etched with HF for 90 min, and (c) SERS spectrum of Crystal Violet of above sample at different points showing the consistency of the substrate with uniform enhancement.**

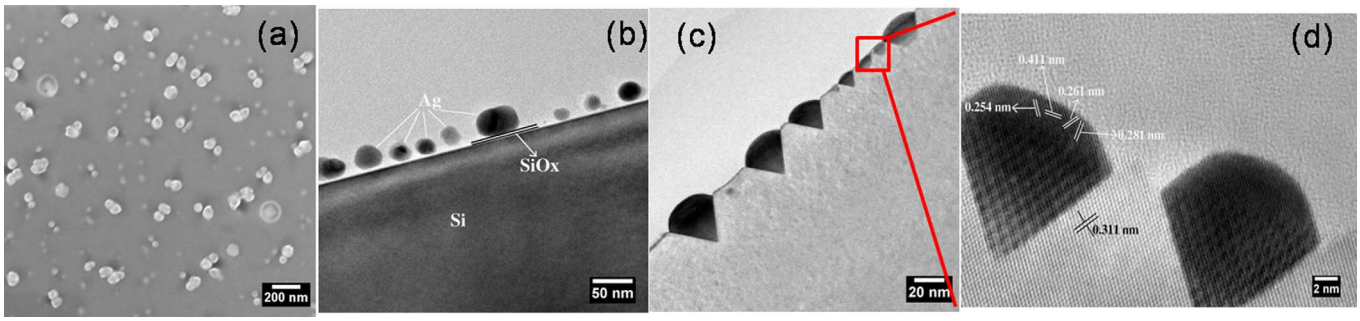

Figure 6 | (a) SEM Micrographs of 2 nm Ag/SiOx/Si (100)@ 800°C in air, X-TEM Micrographs of 2 nm Ag/SiO_x/Si (100)(b) as deposited and annealed at @ 800 °C in air (c) Low Magnification (d) HRTEM of selected area depicts endotaxial structures.

have used a concentration of ≈ 0.5 nM CV while the measurements in ref. 3 are for 5.0 nM. It is expected to have variation in AEF depending on the concentration[3]. It is worth noting that if one could position all the molecules at these hot-spots, then much larger average enhancements could be obtained. Hence, we need to note that the values mentioned here are the average enhancement factors.

In order to look at its reusability, we recorded the SERS spectra with fairly reproducible signals after slightly etching the substrate with HF in the case of CV molecule, as these molecules strongly adhere to the Ag nanoparticles on the substrate through a covalent band. However, if the molecule of interest can easily be removed with a proper solvent, then these substrates can be used several times. The most important thing of robustness is that one does not have to bother about the oxidation of the substrate as Ag particles are covered by SiO_x, GeO_x layers. The second major advantage is that this technique provides the nanostructures that have sharp ordered edges that can be obtained for high field enhancements. The third advantage is that it is highly cost effective.

Role of GeO_x layer. In order to understand the role of GeO_x to form substrate symmetric endotaxial silver nano structures, samples of silver on native oxide silicon substrate are also prepared and annealed at ≈800°C under the same conditions, like 2 nm Ag/17 nm GeO_x/SiO_x/Si(100). Figure 6 (a) is the SEM micrographs of 2 nm Ag/2 nm SiO_x/Si(100) annealed at ≈800°C. Interestingly, no ordered structures have been observed. Figure 6(b) is the low magnification XTEM (cross-sectional TEM) micrograph of as deposited 2 nm Ag/SiO_x/Si(100) revealing the silver nanoparticles on silicon substrate separated by native oxide layer. Figure 6 (c), (d) are the XTEM images of low magnification and high resolution of 2 nm Ag/2 nm SiO_x/Si(100) annealed at ≈800°C in air revealing the intrusion of silver into silicon substrate like 2 nm Ag/17 nm GeO_x/SiO_x/Si(100) @800°C. From the HR-XTEM image, inter planar spacings of 0.254 nm, 0.261 nm, 0.281 nm and 0.411 nm on the structures and 0.311 nm on the substrate have been measured. From these values, 0.254 nm, 0.261 nm are matching with the (131) planes of Ag_2Si, 0.281 nm is matches with the (200) planes of Ag_2Si phase. HR-XTEM images depicts the presence of Moire fringes in the structures, the Moire fringe spacings using Ag_2Si (131) and Si(111) planes with zero angle yielding a value of 1.47 nm, which matches with the measured value 1.46 nm ± 0.02 nm. In this case, formation of Ag_2Si was found within the structures and these structures are also endotaxial in nature (figure 6(d)). This can be explained through the consumption of thermal energy for alloy formation. Mc Brayer et al., reported that silver inter diffuses through SiO_2 layer in the form of Ag^+ ion[37], which will react with the silicon atoms to form alloy at lower temperatures compared to silver atoms. From the observations of 2 nm Ag/2 nm SiO_x/Si(100)@800°C, presence of GeO_x plays a key role in the formation of substrate symmetric single crystalline silver endotaxial nanostructures. We now address the position of GeO_x layer in the formation of these nanostructures.

In order to understand the role of GeO_x position at Ag and Si interface, samples of 17 nm GeO_x/2 nm Ag/2 nm SiO_x/Si were prepared (the Ag layer is sandwiched between GeO_x and SiO_x) and annealed under the same condition as above. Figure 7 (a) is the low magnification X-TEM micrograph of as deposited 17 nm GeO_x/2 nm Ag/2 nm SiO_x/Si(100) shows the irregular Ag structures on top of native oxide are covered along with the inter particle space is filled by GeO_x layer. Figure 7 (b) and (c) are the XTEM micrographs of low magnification and HR-XTEM of 17 nm GeO_x/2 nm Ag/2 nm SiO_x/Si(100) annealed at ≈800°C. XTEM micrograph reveal the formation of embedded Ag nanostructures in the GeO_x layer and the presence of oxide layer in between the silicon substrate and nanostructures. From HR-XTEM image, inter planar distance of 0.239 nm on spherical nano particles which corresponds to Ag (111) plane was measured. Oniki et. al., reported that desorption of GeO_2 into volatile GeO occurs at lower temperatures in presence of metals compared to the absence of metal at the SiO_2/Si interface. This could be one of the possible reasons for the embedded Ag nano structure

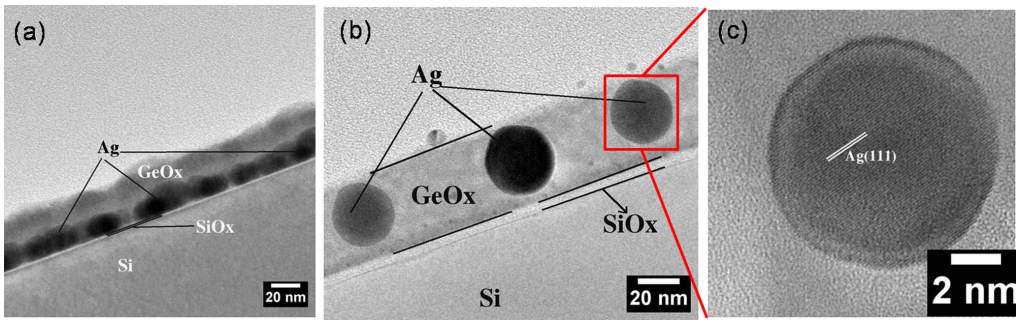

Figure 7 | X-TEM Micrographs of (a) low mag of as deposited 17 nm GeO_x/2 nm Ag/SiO_x/Si (100) (b) Low Mag (c) HR-X-TEM of 17 nm GeO_x/2 nm Ag/SiO_x/Si (100) @ 800°C in air respectively.

formation because of the incomplete desorption of GeO_x within the time and temperature available for the system to react with SiO_x. From above observations it is evident that the position and presence of GeO_x layer plays a key role in the formation of substrate symmetric single crystalline silver endotaxial nanostructures.

Conclusion

Substrate symmetry driven silver nano structures are formed on silicon surface by annealing the 2 nm Ag/17 nm GeO_x/SiO_x/Si samples in ambient conditions at high temperatures. Endotaxial nano squares/rectangles are formed in the case of Si(100), endotaxial nanorods are formed on Si(110) and endotaxial nano triangles are formed for Si(111) substrate according to their 4-fold, 2-fold and 3-fold symmetries respectively. These results show an elegant procedure to fabricate controlled shapes of Ag or Ag_xSi_y endotaxial nanostructures. 3-D structural analysis was carried out using STEM-tomography. These substrates are reusable if the molecules of interest can be removed by a proper solvent without affecting the Ag/Si layer. We believe these endotaxial Ag structures have potential to be robust SERS substrates.

Methods

Silicon wafers of various orientations i.e., (100), (110) and (111) were cleaned by standard procedure of rinsing and sonication with alcohol and de-ionized water. A ≈ 2 nm thick SiO_x (native oxide) layer is also present on all the silicon substrates. Deposition of GeO_x and silver was done by physical vapor deposition (PVD) system. We have used three configurations: (a) a ≈ 17 nm thick GeO_x was deposited on Si(100), Si(110) and Si(111), then the deposition of 2 nm silver was done on 17 nm GeO_x/SiO_x/Si. (b) a ≈ 2 nm thick Ag was deposited on Si followed by GeO_x deposition of about 17 nm thick and (c) a 2 nm thick Ag was deposited on Si. All these three types of samples are annealed in a horizontal tube furnace up to 800°C in atmosphere with a ramp rate of 7°C/minute and hold time is 30 minutes at 800°C. A Carl Zeiss Neon 40 Field Emission Gun Scanning Electron Microscope (FEGSEM) and JEOL JEM-2010 high resolution transmission electron microscope (HRTEM) were used to study the morphology and structure. An FEI Titan 80/300 TEM/STEM microscope operated at 300 keV was used for all STEM measurements. The HAADF detector covered an angular range of 33–200 mrad. For tomography, a single-tilt Fischione tomography sample holder was used and images have been acquired between −66° and +66° of tilt around the substrate surface normal in steps of 2°. The simultaneous iterative reconstruction technique (SIRT) was used for reconstruction with 10 iterations.

Two types of samples (Planar and Cross-sectional) were prepared for TEM observations. For planar samples ≈3 mm disc was cut from the desired sample using ultrasonic disc cutter followed by lapping from the back side to a thickness of ≈100 μm. The disc was dimpled using dimple grinder to a thickness of ≈30 μm at the dimple centre. Electron transparency was achieved using precise ion polishing system (PIPS) with low energy Ar^+ ions. For cross-sectional samples ≈2.5 mm rectangular slabs were cut from the sample and bonded face to face (in order to protect the desired area) using epoxy glue and inserted in a stainless steel (SS) tube of inner diameter of ≈2.5 mm and outer diameter of ≈3 mm using epoxy glue. A ≈500 μm thick disc is cut from the above packed SS tube using diamond wheel saw. This disk is lapped from both the sides to a thickness of ≈100 μm, which is polished from both sides and dimpled from one side to a thickness of ≈30 μm at dimple centre. Electron transparency was achieved using 6.0 keV energy Ar^+ ions.

Samples (2 nm Ag/17 nm GeO_x/SiO_x/Si(100) @ 800°C) were cleaned using Piranha solution for 30 minutes and dipped in 5% Hydroflouric acid for 90 minutes to remove the top oxide layers. After removing from the HF solution samples were allowed to dry in air for 30 minutes and then C V solution with various concentrations was drop casted on top of the substrate. SERS spectra were recorded using micro-Raman spectrometer (LABRAM-HR) using laser excitation lines of 514.5 nm at room temperature. The reason for recording SERS spectra with this excitation wave length was to study resonance of adsorbate on Ag nanostructures. All the measurements were made in a backscattering geometry, using a 50× microscope objective lens with a numerical aperture of 0.7. Typical laser power at the sample surface was ≈1.0 mW with a spot size of ≈2 μm. A 20 μl of the CV solution (5×10^{-10} M) was dropped onto the SERS substrate and allowed it to dry naturally. A fixed volume micro-pipette with disposable tips was used to prevent contamination. In our tests the dropped solution soon spread over the whole SERS substrate but remained confined to the substrate. Synchrotron based x-ray diffraction measurements have been carried out at BL-18B, Photon Factory (PF), KEK using 11.38 keV x-rays and with a beam size of 250 μm × 250 μm.

1. Kneipp, J., Kneipp, H., Wittig, B. & Kneipp, K. Novel optical nanosensors for probing and imaging live cells. *Nanomed.: Nanotech. Bio. Med.* **6**, 214–226 (2010).
2. Stiles, P. L., Dieringer, J. A., Shah, N. C. & Van Duyne, R. P. Surface-Enhanced Raman Spectroscopy. *Annu. Rev. Anal. Chem.* **1**, 601–626 (2008).
3. Le Ru, E. C., Blackie, E., Meyer, M. & Etchegoin, P. G. Surface Enhanced Raman Scattering Enhancement Factors: A Comprehensive Study. *J. Phys. Chem. C* **111**, 13794–13803 (2007).
4. Qian, X. M. & Nie, S. M. Single-Molecule and Single-Nanoparticle SERS: from Fundamental Mechanisms to Biomedical Applications. *Chem. Soc. Rev.* **37**, 912–920 (2008).
5. Sharma, B., Frontiera, R. R., Henry, A. I., Ringe, E. & Van Duyne, R. P. SERS: Materials, Applications and the Future. *Materials Today* **15**, 16–25 (2012).
6. Otto, A. What is observed in single molecule SERS, and why? *J. Raman Spectroscopy* **33**, 593–598 (2002).
7. Camaden, J. P. *et al.* Probing the Structure of Single-Molecule Surface-Enhanced Raman Scattering Hot Spots. *J. Am. Chem. Soc.* **130**, 12616–12617 (2008).
8. Stender, A. S. *et al.* Single Cell Optical Imaging and Spectroscopy. *Chem. Rev.* **113**, 2469–2527 (2013).
9. Schultz, S., Smith, D., Mock, J. J. & Schultz, D. A. Single Target Molecule Detection with Nonbleaching Multicolor Optical Immunolabels, Proc. *Natl. Acad. Sci., USA* **97**, 996–1001 (2000).
10. Anker, J. N. *et al.* Biosensing with Plasmoic Nanoosensors. *Nat. Mater.* **7**, 442–453 (2008).
11. Wustho lz, K. L. *et al.* Structure−Activity Relationships in Gold Nanoparticle Dimers and Trimers for Surface-Enhanced Raman Spectroscopy. *J Am Chem. Soc.* **132**, 10903–10910 (2010).
12. Negri, P. & Dluhy, R. A. Ag nanorod based surface-enhanced Raman spectroscopy applied to bioanalytical sensing. *J. Biophotonics* **6**, 20–35 (2013).
13. Naya, M., Tani, T., Tomaru, Y., Li, J. & Murakami, N. Nanophotonics bio-sensor using gold nanostructure. *Proc SPIE* **7032**, 70321Q/1 (2008).
14. Fang, J., Liu, S. & Li, Z. Polyhedral silver mesocages for single particle surface-enhanced Raman scattering-based biosensor. *Biomaterials* **32**, 4877–4884 (2011).
15. Biggs, K. B., Camden, J. P., Anker, J. F. & Van Duyne, R. P. Surface-Enhanced Raman Spectroscopy of Benzenethiol Adsorbed from the Gas Phase onto Silver Film over Nanosphere Surfaces: Determination of the Sticking Probability and Detection Limit Time. *J. Phys. Chem. A* **113**, 4581–4586 (2009).
16. Barnes, W. L., Dereux, A. & Ebbesen, T. W. Surface plasmon subwavelength optics. *Nature* **424**, 824–830 (2003).
17. Hu, X. & Chan, C. T. Photonic Crystals with Silver Wires as a Near-Infrared Superlens. *Appl. phys. lett.* **85**, 1520–1522 (2004).
18. Pang, Y. T., Meng, G. W., Fang, Q. & Zhang, L. D. Silver Nanowire Array Infrared Polarizers. *Nantechnology.* **14**, 20–22 (2003).
19. Wiley, B., Sun, Y. & Xia, Y. Synthesis of Silver Nanostructures with Controlled Shapes and Properties. *Acc. Chem. Res.* **40**, 1067–1076 (2007).
20. Juluri, R. R., Rath, A., Ghosh, A. & Satyam, P. V. Substrate Symmetry Driven Endotaxial Silver Nanostructures by Chemical Vapor Deposition. *J. Phys. Chem. C.* **117**, 13247–13251 (2013).
21. Bonev, I. On the Terminology of the Phenomena of Mutual Crystal Orientation. *Acta. Cryst. A* **28**, 508–512 (1972).
22. Bennet, P. A., He, Z., Smith, D. J. & Ross, F. M. Endotaxial Silicide Nanowires: A Review. *Thin Solid films* **519**, 8434–8440 (2011).
23. Williams, D. B. & Carter, C. B. Transmission Electron Microscopy: A Textbook for Materials Science (Springer, 1996).
24. Oniki, Y., Koumo, H., Iwazaki, Y. & Ueno, T. Evaluation of GeO Desorption Behavior in the Metal/GeO_2/Ge Structure and Its Improvement of the Electrical Characteristics. *J. Appl. Phys.* **107**, 124113-1–124113-5 (2010).
25. Kamata, Y., Takashima, A. & Tsutomu, T. Material Properties, Thermal Stabilities and Electrical Characteristics of Ge MOS Devices, Depending on Oxidation States of Ge Oxide: Monoxide [GeO(II)] and Dioxide [GeO_2(IV)]. *Mat. Res. Soc. Symp. Proc.* **1155**, C02–04 (2009).
26. Bernstein, R. B. & Cubicciotti, D. The Kinetics of the Reaction of Germanium and Oxygen. *J. Am. Chem. Soc.* **73**, 4112–4114 (1951).
27. Wang, S. K., Liu, H. G. & Toriumi, A. Kinetic study of GeO Disproportiantion into GeO_2/Ge System using X-ray Photoelectron Spectroscopy. *Appl. Phys. Lett.* **101**, 061907-1–061907-4 (2012).
28. Yun, S. J., Lee, S. C., Kim, B. & Kang, S. W. Study of Interaction between Incident Silicon and Germanium Fluxes and SiO_2. *J. Vac. Sci. Technol., B* **12**, 1167–1169 (1994).
29. Nason, T. C., Yang, G. R., Park, K. H. & Lu, T. M. Study of Silver DIffusion into Si(111) and SiO_2 at Moderate Temperature. *J. Appl. Phys.* **70**, 1392–1396 (1991).
30. Rollert, F., Stolwijk, N. A. & Mehrer, H. Solubility, Diffusion and Thermodynamic Properties of Silver in Silicon. *J. phys. D: Appl. Phys.* **20**, 1148–1155 (1987).
31. Xin, H., Zhang, J.-M., Wei, X.-M. & Xu, K. W. Anisotropy Analysis of Energy in Ag/Si Twist Interface. *Surf. and Inter. Anal.* **37**, 608 (2005).
32. Wulff, G. Zur Frage der Geschwindigkeit des Wachsthums und der Auflosung der Krystallflachen. *Zeitschrift für Krystallographie und Mineralogie* **34**, 449 (1901).
33. Laue, M. v. Der Wulffsche Satz fur die Gleidigewichtsform von Kristallen. *Zeitschrift für Kristallographie* **105**, 124 (1943).
34. Leopold, N. & Lendl, B. A New Method for Fast Preparation of Highly Surface-Enhanced Raman Scattering (SERS) Active Silver Colloids at Room Temperature by Reduction of Silver Nitrate with Hydroxylamine Hydrochloride. *J. Phys. Chem. B* **107**, 5723–5727 (2003).
35. Kneipp, K. *et al.* Single Molecule Detection Using Surface-Enhanced Raman Scattering (SERS). *Phys. Rev. Lett.* **78**, 1667–1670 (1997).

36. Cho, W. J., Kim, Y. & Kim, J. K. Ultrahigh-Density Array of Silver Nanoclusters for SERS Substrate with High Sensitivity and Excellent Reproducibility. *ACS Nano* **6**, 249–255 (2012).
37. Mc Brayer, J. D., Swanson, R. M., Sigmon, T. W. & Bravman, J. Observation of Rapid Field Aided Diffusion of Silver in Metal Oxide Semiconductor Structures. *Appl. Phys. Lett.*, **43**, 653–654 (1983).

Acknowledgments

Prof PVS's work has been funded by the Department of Atomic Energy, Government of India for project No. 12-R&D-IOP-5.09-0100 for whole project. The authors acknowledge Department of Science and Technology, India for the financial support and Saha Institute of Nuclear Physics, India for facilitating the experiments at the Indian Beamline, Photon Factory, KEK, Japan. DNR's work has been funded by Department of Science and Technology – ITPAR – Phase – 3 project and RS's work has been funded by Department of Science and Technology PURSE Fellowship.

Author contributions

R.R.J., A.Rath and P.V.S. took part in conceiving the idea, performed experiments, and R.R.J. and P.V.S. wrote the main manuscript; A.G. and A.B. took part in the growth of the samples and preparation of the specimen; R.S. and D.N.R. took performed the Raman measurements and wrote part of the manuscript; K.M., M.S., K.F., T.G., F.K. and A.R., performed STEM measurements, STEM-Tomography measurements and wrote part of the manuscript. All authors reviewed the manuscript.

Additional information

Competing financial interests: The authors declare no competing financial interests.

How to cite this article: Juluri, R.R. *et al*. Coherently Embedded Ag Nanostructures in Si: 3D Imaging and their application to SERS. *Sci. Rep.* **4**, 4633; DOI:10.1038/srep04633 (2014).